AJNR

High-Resolution MR Cisternography of the Cerebellopontine Angle: 2D versus 3D Fast Spin-Echo Sequences

Eriko Iwayama, Shinji Naganawa, Tokiko Ito, Hiroshi Fukatsu, Mitsuru Ikeda, Takeo Ishigaki and Nobuyasu Ichinose

AJNR Am J Neuroradiol 1999, 20 (5) 889-895
http://www.ajnr.org/content/20/5/889

AJNR Am J Neuroradiol 20:889–895, May 1999

High-Resolution MR Cisternography of the Cerebellopontine Angle: 2D versus 3D Fast Spin-Echo Sequences

Eriko Iwayama, Shinji Naganawa, Tokiko Ito, Hiroshi Fukatsu, Mitsuru Ikeda, Takeo Ishigaki, and Nobuyasu Ichinose

BACKGROUND AND PURPOSE: **The clinical usefulness of MR cisternography of the cerebellopontine angle, applying 2D or 3D fast spin-echo sequences, has been reported recently. Our purpose was to investigate the cause of signal loss in CSF in the prepontine or cerebellopontine angle cistern on 2D FSE MR images and to compare the cisternographic effects of 2D and 3D FSE sequences.**

METHODS: **Preliminary experiments were performed in four volunteers to assess the causes of signal loss. Initially, using a 2D cardiac-gated cine phase-contrast method with a velocity encoding value of 6 cm/s, we measured the velocity and flow pattern of CSF. Comparisons were made to assess the effects of intravoxel dephasing, amplitude of the section-selecting gradient, echo time (TE), and section thickness. Four healthy subjects and 13 patients with ear symptoms were examined, and multisection 3-mm-thick 2D images and 30-mm-slab, 1-mm-section 3D images were compared qualitatively and quantitatively. Then, 3D MR cisternography was performed in 400 patients with ear symptoms, and qualitative evaluation was performed.**

RESULTS: **In volunteers, the average peak velocity of CSF was 1.2 cm/s. With TE = 250, CSF may move an average of 3 mm, and can be washed out of a 3-mm-thick 2D section volume. The CSF signal relative to that of a water phantom decreased gradually as TE increased on single-section 3-mm-thick 2D images. The CSF signal relative to that of the water phantom increased gradually as section thickness increased. No significant differences were noted in intravoxel dephasing and amplitude of the section-selecting gradient. The contrast-to-noise ratio (CNR) between CSF and the cerebellar peduncle, and the visibility of the cranial nerves and vertebrobasilar artery were significantly improved on 3D images in 17 subjects. In images from 400 patients, no significant signal loss in the cistern was observed using 3D FSE.**

CONCLUSION: **CSF signal loss in thin-section 2D MR cisternography is mainly attributable to the wash-out phenomenon. 3D acquisition can reduce this phenomenon and provide thinner sections. The scan time for 3D acquisition is not excessive when a long echo train length and half-Fourier imaging are used. MR cisternography should be performed using a 3D acquisition.**

The clinical utility of MR cisternography of the cerebellopontine angle and internal auditory canal (IAC) using heavily T2-weighted images acquired by 2D (1–8) or 3D (9–15) fast spin-echo (FSE) sequences has recently been reported. In thin-section 2D MR cisternography, we frequently encounter signal loss in CSF in the prepontine or cerebellopontine angle cistern, which degrades the cisternographic effect. The diagnosis of acoustic neuroma and visualization of the IAC structure depend on contrast between high-signal-intensity CSF and low-signal-intensity structures. A reduction in CSF signal, therefore, reduces this contrast. The cause of signal loss in the cistern on 2D thin-section images has been hypothesized to be due to pulsation ghosts of CSF, the wash-out phenomenon, or dephasing by the strong amplitude of the section-selecting gradient (8). Pulsation ghosts of CSF are caused by the CSF periodic movement during the cardiac cycle. The wash-out phenomenon is caused by the outflow of excited spins from the volume of interest before receiving 180° pulses for

Received August 21, 1998; accepted after revision January 15, 1999.

From the Department of Radiology, Nagoya University School of Medicine, Nagoya (E.I., S.N., T.It., H.F., M.I., T.Is.); and Toshiba Corporation, Tokyo (N.I.), Japan.

Address reprint requests to Eriko Iwayama, MD, Department of Radiology, Nagoya University School of Medicine, 65 Tsurumai-cho, Shouwa-ku, Nagoya 466-8550, Japan.

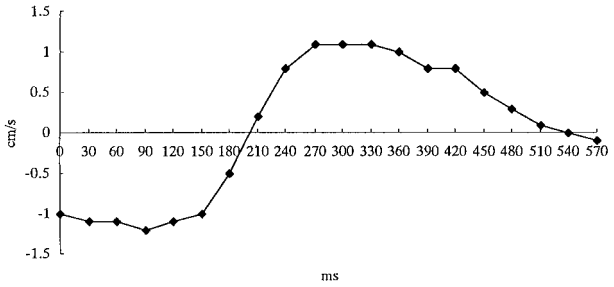

FIG 1. Flow velocity and flow pattern of CSF in the prepontine cistern obtained in a volunteer with cine phase velocity mapping. The average peak velocity of CSF in four volunteers was 1.2 cm/s.

Table 1: The peak velocity (cm/s) of CSF in four volunteers

	Volunteers			
	A	B	C	D
Maximum	1.1	1.1	1.3	1.3
Minimum	−1.2	−0.9	−0.1	−0.6

Note.—The average peak velocity of CSF was 1.2 cm/s.

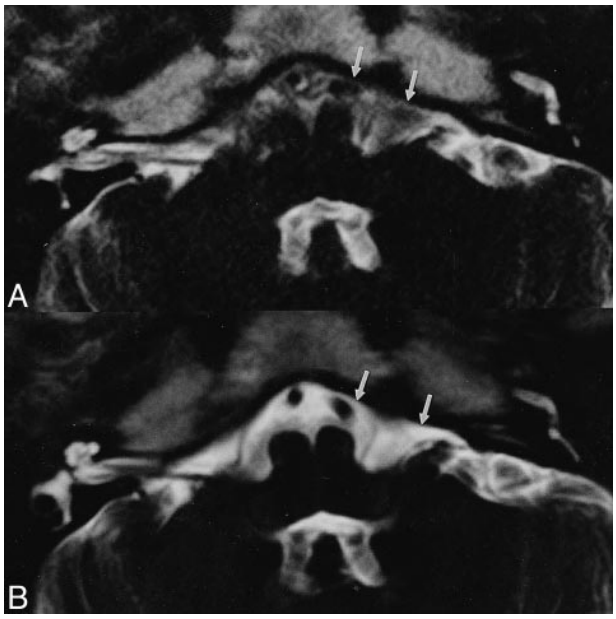

FIG 2. *A* and *B*, Single-section 3-mm-thick 2D image (*A*) and 30-mm-slab 3-mm-section 3D image (*B*). The 2D image shows loss of signal intensity in the prepontine cistern (*arrows*) compared with the 3D image (*arrows*).

Table 2: Relative signal intensity* on single-section 3-mm-thick 2D images, 30-mm-slab 3-mm-section 3D images, 30-mm-slab 3D images with intraslab presaturation pulses except in the 1-mm-slab center volume, and 30-mm-slab 1-mm-section 3D images without a presaturation pulse in four volunteers

	Volunteers					
	A	B	C	D	Average ± SD	
2D-3-mm	0.24	0.59	0.32	0.64	0.45 ± 0.20	$P < .05$
3D-3-mm	0.66	0.78	0.72	0.67	0.71 ± 0.10	NS
3D-1-mm without saturation pulse	0.55	0.71	0.70	0.73	0.67 ± 0.08	$P < .01$
3D-1-mm with saturation pulse	0.19	0.44	0.21	0.36	0.30 ± 0.12	

Note.—SD indicates standard deviation; NS, no significant difference.
* Signal intensity of CSF/signal intensity of water phantom.

refocusing, especially at the effective echo time (TE) in fast spin-echo sequences. Dephasing by the section-selecting gradient is caused by the spin dephasing due to the movement along the strong section-selecting gradient for 2D thin-section images. The purpose of this study was to investigate the cause of this signal loss and to compare the cisternographic effects of 2D and 3D FSE sequences.

Methods

Preliminary experiments were performed in four volunteers to investigate the cause of signal loss. All experiments were performed using a 1.5-T MR system with a quadrature head coil. Imaging parameters, except for section thickness and the number of sections, were kept constant during all experiments to permit accurate comparison as follows: 4000/250 (TR/TE_{eff}), a field of view of 21 cm, an in-plane matrix of 384 × 384, an echo train length of 68, and echo spacing of 12.5 milliseconds. The scan time was 8 minutes 36 seconds. The number of excitations was adjusted to obtain the same signal-to-noise ratio (SNR) in 2D and 3D images. During the preliminary experiments, a water phantom was placed near the external auditory meatus.

Preliminary Experiments

Initially, using 2D cardiac-gated cine phase-contrast acquisition with a velocity-encoding value of 6 cm/s, the velocity and flow pattern of CSF were measured. Parameters of 30/16 (TR/TE) and a flip angle of 20° were applied.

Various comparisons were made as follows: maintaining the slab thickness at 30 mm, we compared 1-mm-section 3D and 3-mm-section 3D images to assess the effects of intravoxel dephasing by changing the voxel size. The relative signal intensity (RSI) of CSF in the cistern at the mid-portion between the vertebral artery and the entrance to the IAC against the water phantom was calculated. The region of interest (ROI) specified was greater than 3 mm in diameter. The RSI was given as an equation: RSI = signal intensity of CSF/signal intensity of water phantom.

Single-section 3-mm-thick 2D images and 30-mm-slab 3-mm-section 3D images were compared to assess the difference between 2D and 3D acquisitions with the same voxel size. RSI was calculated. To evaluate the wash-out phenomenon, differences in the dephasing effect due to the section-selecting gra-

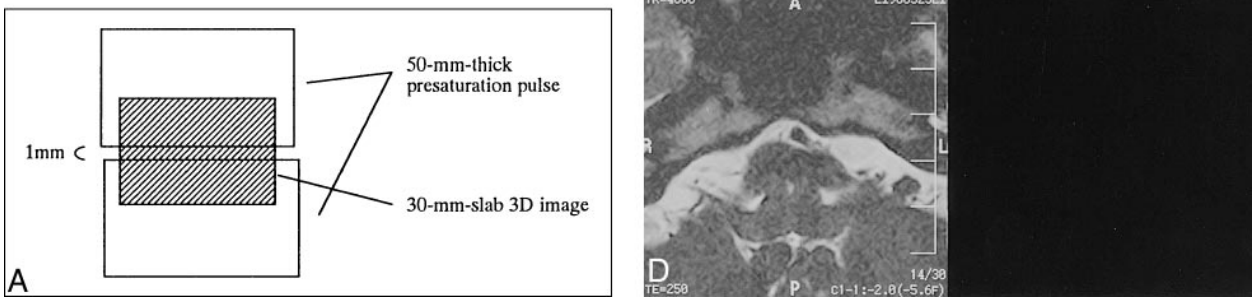

FIG 3. *A,* Schematic diagram of 30-mm-slab 3D images (*shaded area*) with intraslab presaturation pulses except for the 1-mm-slab center volume.
B, 30-mm-slab 1-mm-section 3D image with intraslab presaturation pulses show signal loss (*arrows*).
C, Single-section 3-mm-thick 2D image shows some signal loss (*arrowheads*).
D, 30-mm-slab 1-mm-section 3D image without presaturation pulse shows no signal loss in the prepontine cistern.

dient between 2D and 3D acquisitions were excluded by obtaining the following: 30-mm-slab 3D images with intraslab presaturation pulses except in the 1-mm-slab center volume, 30-mm-slab 1-mm-section 3D images without a presaturation pulse, and single-section 3-mm-thick 2D images. Because the slab profiles are not perfectly sharp-edged, they are likely to saturate part of the signal both for CSF and the water phantom in the center of the slab even if they are specified not to saturate that volume. Thus, to evaluate whether the signal loss due to saturation pulses in flowing CSF is greater than that in the stationary water of the phantom, the RSI was calculated by placing the water phantom in the same manner as in the other preliminary experiments. Comparison was carried out for various TE values on single-section 3-mm-thick 2D images (TE = 80, 100, 120, 160, and 254). RSI was calculated. Furthermore, the CNR between the water phantom and the cerebellar peduncle was calculated. CNRs were measured by setting ROIs in the cerebral cistern at the mid-portion between the vertebral artery and the entrance to the IAC, in the cerebellar peduncle, and in air outside the zygomatic bone.

A comparison was made of the various section thicknesses for single-section 2D images (2, 3, 4, and 5 mm), and RSI was calculated.

Clinical Evaluation

In four healthy subjects and 13 patients with ear symptoms, multisection 3-mm-thick 2D and 30-mm-slab 1-mm-section 3D images were compared. No saturation pulses were applied. CNRs in CSF and in the cerebellar peduncle were measured quantitatively. The visibility of the vertebrobasilar artery, vestibulocochlear nerve, and trigeminal nerve were scored qualitatively. The visibility scores were assigned independently by two radiologists. If there was a difference between the two scores, consensus was achieved by discussion. The scores were 0, 1, 2, and 3, corresponding to poor (impossible to recognize the anatomic structure because of marked signal loss in CSF), fair (possible to recognize the anatomic structure despite obvious signal loss in CSF), good (easy to recognize the anatomic structure although some signal loss in CSF was noted), and excellent (no signal loss in CSF), respectively. 3D MR cisternography was then performed in 400 patients with ear symptoms, and qualitative evaluation was performed using the same method as for 2D imaging.

Statistical Analysis

Statistical analysis in regard to RSI and CNR was performed with the paired Student's *t*-test, and statistical analysis with regard to a comparison of visibility scores was performed using the Wilcoxon signed-rank test.

Results

Preliminary Experiments

The average peak velocity of CSF was 1.2 cm/s (Fig 1 and Table 1). Based on analysis of the flow pattern, CSF may move an average of 3 mm during a TE of 250. With a TE of 250 or longer, CSF can therefore be washed out of a 3-mm-thick 2D section volume at the TE of 250. No significant changes in signal intensity were found between 30-mm-slab 1-mm-section 3D images and 3-mm-thick 3D images, and no effects related to intravoxel dephasing were detected (Table 2). Using the same voxel size, we found that 3D images showed higher CSF signal intensity than 2D images (Fig 2). RSI was significantly higher on 3D images ($P < .05$) (Table 2). The 30-mm-slab 3D images with presaturation pulses showed signal loss (Fig 3). RSI was significantly lower on 3D images with presaturation pulses than without presaturation pulses ($P < .01$) (Table 2), meaning that the effect of saturation pulses on CSF is greater than that on a water phantom. RSI decreased gradually as TE increased in

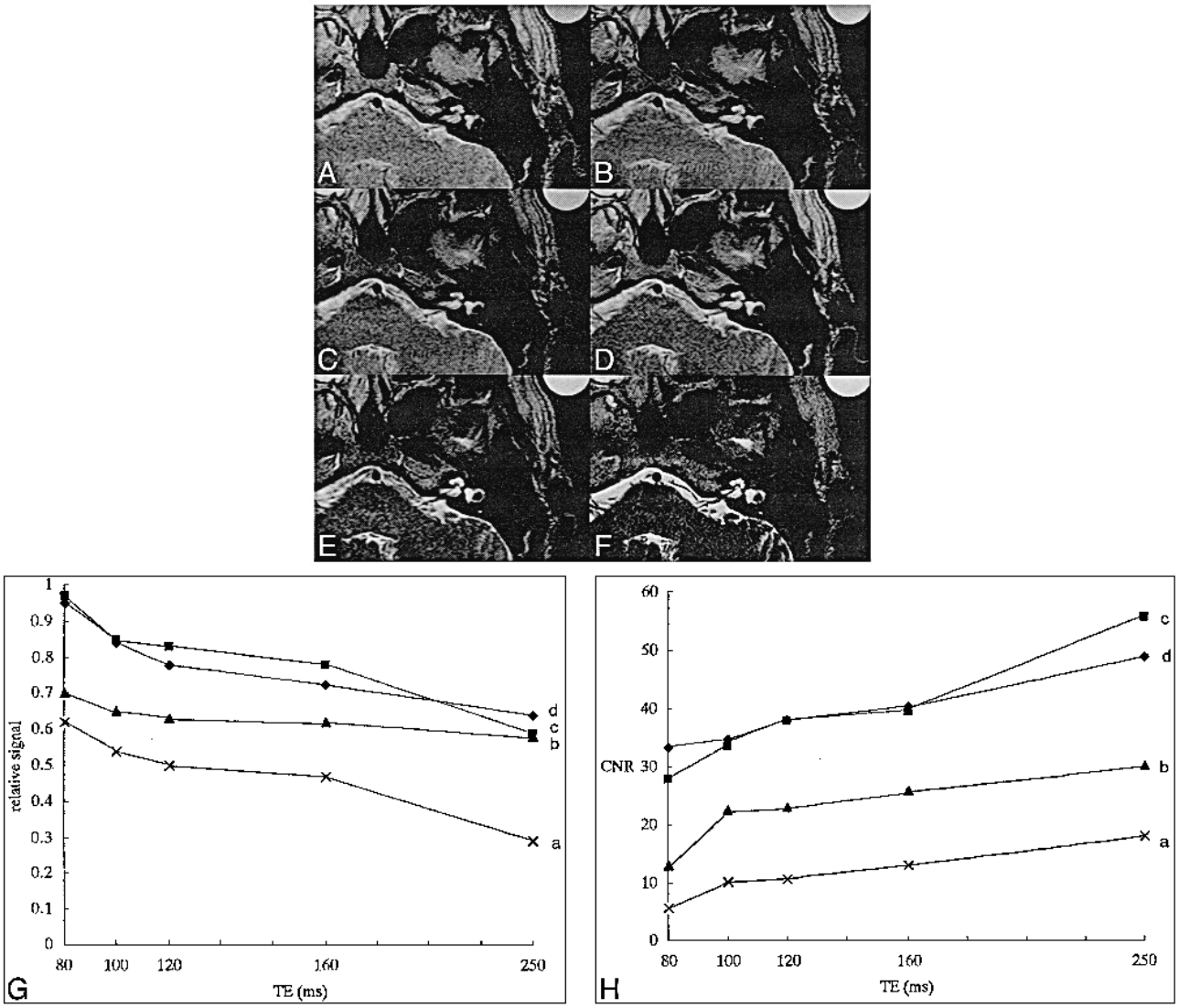

FIG 4. *A–H,* Comparison of various TEs in single-section 3-mm-thick 2D images: TE = 80 (*A*), TE = 100 (*B*), TE = 120 (*C*), TE = 160 (*D*), TE = 254 (*E*); and 30-mm-slab 1-mm-section 3D image (*F*). In all four volunteers, CSF signal relative to that of the water phantom decreased gradually as TE increased in single-section 3-mm-thick 2D images (*G*). In all four volunteers, CNR between the water phantom and the cerebellar peduncle increased gradually as TE increased (*H*).

single-section 3-mm-thick 2D images. However, CNR between the water phantom and the cerebellar peduncle increased gradually as TE increased (Fig 4). RSI increased gradually as section thickness increased (Fig 5).

Clinical Evaluation

CNR between CSF and the cerebellar peduncle in 17 subjects was significantly higher on 3D images (2D: 18.4 ± 7.5; 3D: 40.0 ± 19.3; $P < .05$) (Fig 6). On 2D images, the visibility scores for the vertebrobasilar artery, vestibulocochlear nerve, and trigeminal nerve were lower than those on 3D images (Table 3). The visibility scores for these structures were significantly higher on 3D images ($P < .001$). In an exceptional case, on 2D images, the signal loss within CSF adjacent to the epidermoid cyst provided contrast not visible on 3D images (Fig 7).

In all images obtained in the 400 patients with ear symptoms, the visibility grading of the vertebrobasilar artery, vestibulocochlear nerve, and trigeminal nerve was either excellent or good (Table 4). In no instance was visualization considered fair or poor.

Discussion

The clinical utility of MR cisternography in the cerebellopontine angle and the IAC using heavily T2-weighted images acquired by 2D FSE (1–8) or 3D FSE (9–15) has recently been reported. Because the CSF and fluid in the inner ear have long T2 values, when a long TR and a long TE are used, these fluid-filled structures have high signal inten-

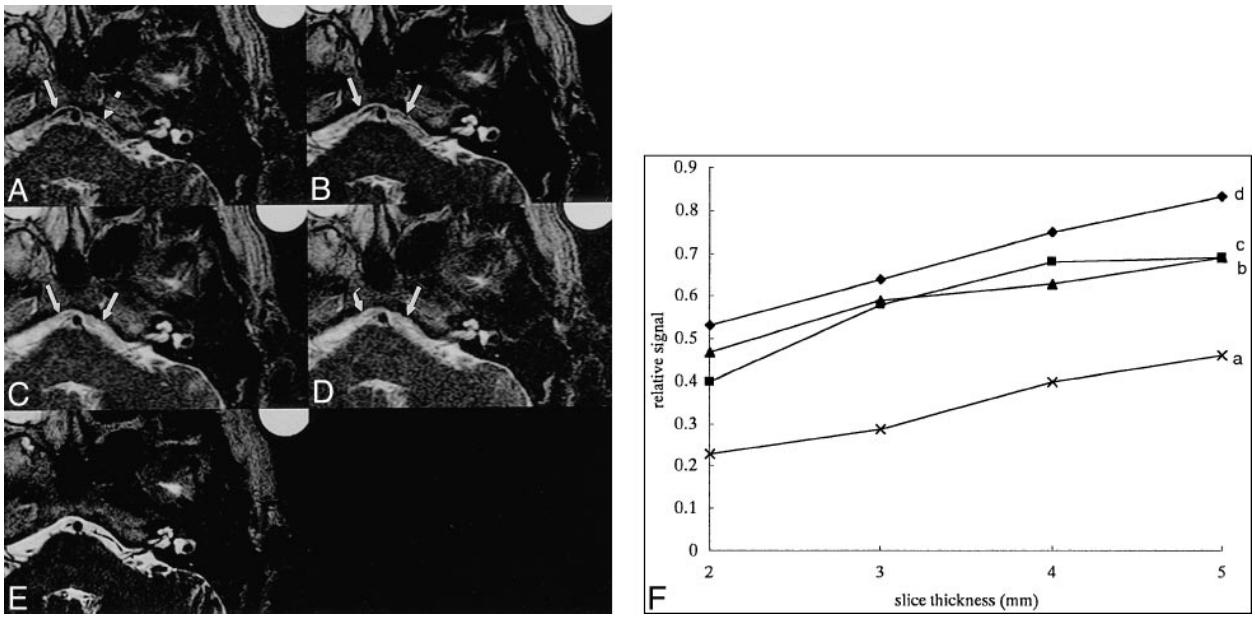

FIG 5. *A–F,* Comparison of various section thicknesses for single-section 2D images: 2 mm (*A*), 3 mm (*B*), 4 mm (*C*), 5 mm (*D*); and 30-mm-slab 1-mm-section 3D image (*E*). In all four volunteers, CSF signal relative to that of the water phantom increased gradually as section thickness increased (*arrows* in *A–E*) (*F*).

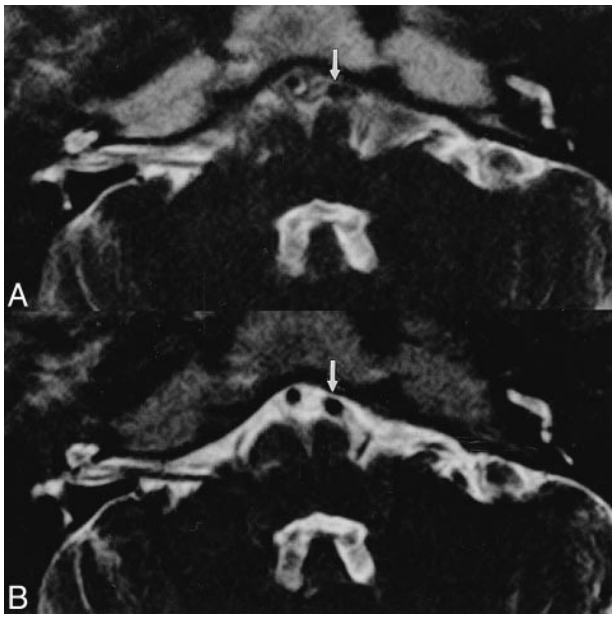

FIG 6. Images obtained in a healthy volunteer for comparison of 2D and 3D FSE sequences.

A, Multisection 3-mm-thick 2D image.

B, 30-mm-slab 1-mm-section 3D image. The visibility of the vertebral artery is poor in the 2D image (*arrow*) but excellent in the 3D image (*arrow*).

Table 3: The visibility grading of vertebrobasilar artery, vestibulocochlear nerve, and trigeminal nerve as seen on 2D versus 3D images (n = 17)

	2D	3D
Vertebrobasilar artery		
Excellent	1	16
Good	4	1
Fair	9	0
Poor	3	0
Vestibulocochlear nerve		
Excellent	6	17
Good	7	0
Fair	2	0
Poor	2	0
Trigeminal nerve		
Excellent	6	16
Good	6	1
Fair	5	0
Poor	5	0

Note.—The visibility scores for these structures were significantly higher on 3D images ($P < .001$).

sity, while most other tissues, such as cranial nerves, vessels, and IAC masses, appear hypointense relative to CSF (2). Thus, signal loss in the CSF interferes with the visualization of structures in the cerebral cisterns and IAC.

The 3D gradient-echo (GRE) and steady-state free precession (SSFP) techniques have been used to examine the inner ear (3, 9, 10, 12). However, the high sensitivity to motion and magnetic susceptibility artifacts of these sequences decrease the signal intensity of the CSF in the vicinity of the cerebellopontine angle, resulting in low contrast between soft tissues and CSF (9). Magnetic susceptibility artifacts, which are inherent to the 3D GRE technique, are especially prominent in the temporal bone region, where small soft-tissue structures interface with surrounding bone and air (3).

The FSE sequence is less sensitive to magnetic susceptibility artifacts and allows the visualization of tiny structures in the inner ear (9). Although a long TR/TE 2D FSE sequence also provides high signal intensity for the CSF/perilymph/endolymph,

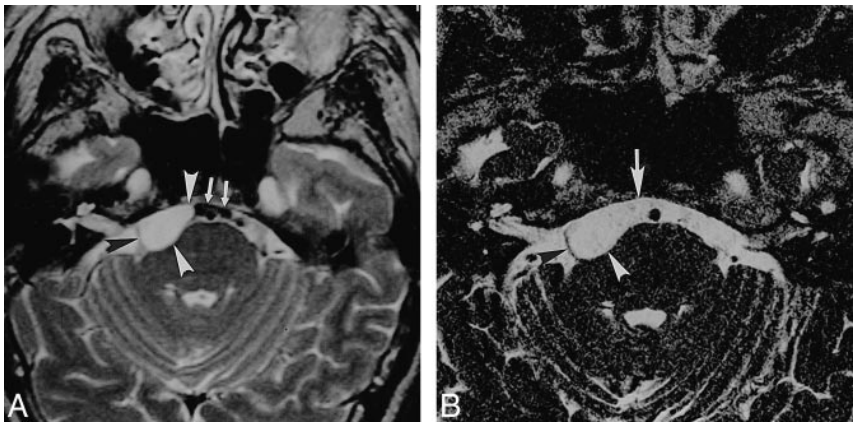

FIG 7. 57-year-old man with right-sided trigeminal neuralgia.

A and *B*, Multisection 3-mm-thick 2D image (*A*) and 30-mm-slab 1-mm-section 3D image (*B*). A mass (*white arrowheads*) presumed to be an epidermoid cyst compressing the trigeminal nerve (*black arrowheads*) is depicted in the right cerebellopontine angle. Although the tumor is isointense with CSF on the 3D image (*large arrow*), the tumor can be recognized more clearly on the 2D image, owing to signal loss in CSF (*small arrows*).

Table 4: The visibility grading of vertebrobasilar artery, vestibulocochlear nerve, and trigeminal nerve on 3D images (n = 400)

Vertebrobasilar artery	
Excellent	352
Good	48
Fair	0
Poor	0
Vestibulocochlear nerve	
Excellent	400
Good	0
Fair	0
Poor	0
Trigeminal nerve	
Excellent	400
Good	0
Fair	0
Poor	0

it sometimes causes prominent signal loss in the CSF, and its 2- to 3-mm section thickness is not completely satisfactory for inner ear studies (9). The reason for the signal loss in CSF in the cerebral cisterns has been hypothesized to be due to pulsation ghosts, the wash-out phenomenon from the thin-section volume, or dephasing by the strong amplitude of the section-selecting gradient (8); however, consensus has not yet been reached (9). To our knowledge, no previous study has been conducted systematically to address this question. On thin-section 2D images, CSF ghosts were not identified in the phase-encoding direction; thus, this is not likely to be the main reason for the signal loss. Differences in the dephasing effect due to the section-selecting gradient between 2D and 3D acquisition were excluded by imaging the slab with and without intraslab presaturation pulses, except in the 1-mm-slab center volume. In this experiment, the slab-selective gradient was the same and the effective excitation volume was 30 mm without saturation pulses and 1 mm with saturation pulses. Thus, excitation of a thick volume and a thin volume were compared without changing the amplitude of the section-selecting gradient. Although intravoxel dephasing can also be a cause of CSF signal loss, 3D acquisition images showed better cisternographic effects than 2D images, even with the same voxel size. Intravoxel dephasing is therefore not a main cause of the signal loss in CSF. Images obtained with thicker sections and shorter TEs showed better cisternographic effects. These results also support the contention that the main cause of signal loss in the CSF on thin-section 2D MR cisternography is movement of CSF from the section of excitation prior to signal measurement (wash-out phenomenon).

Generally, the loss of signal in CSF interferes with the diagnosis of cerebellopontine angle lesions. However, epidermoid cysts appear bright on T2-weighted images, are isointense with CSF, and are difficult to recognize on 3D FSE sequences (16). Signal loss in the CSF on 2D FSE images facilitated the recognition of epidermoid cysts, eliminating the need to perform further examinations in this uncommon condition. On 3D FSE images, the visualization of small intracanalicular acoustic tumors may be possible without the use of paramagnetic contrast material (3, 9, 10, 11, 13). Owing to thin-section capabilities, the 3D FSE method permits visualization of the relationship between the tiny, tortuous vessels and the cranial nerves in the vicinity of the IAC. This method may therefore be helpful in the diagnosis of neurovascular compression (9, 10, 13).

Another advantage of the 3D method is the ability to obtain maximum-intensity projections, which may prove useful in the evaluation of complex 3D structures, such as the inner ear. 3D constructive interference in steady state (CISS) can also be applied to MR cisternography. In our experience, 3D CISS images of the internal carotid artery and basilar artery can show either high signal or low signal depending on its position in the slab. This may decrease the value of 3D MR cisternography using 3D CISS; however, this will require future studies that directly compare image quality obtained with the 3D CISS and 3D FSE methods (9, 17, 18).

With a half-Fourier imaging technique, slightly more than half the k-space data are acquired, then the image is reconstructed; thus, scan time may be shortened by nearly 50% (11). The drawback of the

half-Fourier technique is a lower SNR as compared with the conventional Fourier technique. The time saved can be used either to obtain a higher spatial resolution or simply to reduce the patient scan time (11). For example, an IAC screening study can be performed in fewer than 3 minutes (11). In this experiment, to include the phantom near the external auditory meatus, the field of view was set at 21 cm, which is larger than the 15 cm used in the routine IAC screening protocol. To maintain the spatial resolution, a 384 × 384 matrix was applied instead of the typical 256 × 256 matrix. This resulted in the longer scan time in this experiment. We imaged 400 patients with 3D MR cisternography without experiencing significant signal loss, supporting the excellence of 3D MR cisternography in the clinical setting. The information obtained in this study may also prove useful for identifying the cause of signal loss in 2D axial MR myelography (19, 20).

Conclusion

The signal loss in CSF in thin-section 2D MR cisternography can be attributed mainly to the wash-out phenomenon. The 3D acquisition can reduce this phenomenon and provide thinner sections. Use of a long echo train length and a half Fourier imaging technique in 3D FSE allows for inner ear MR studies with a tremendous time reduction and high spatial resolution without significant penalty. We conclude that MR cisternography should be performed with a 3D FSE acquisition.

References

1. Swarz JR. **Sensorineural hearing deficit: a systematic approach of the vestibular nerve.** *Arch Otolaryngol* 1975;101:91–95
2. Fukui MB, Weissman JL, Curtin HD, Kanal E. **T2-weighted MR characteristic of internal auditory canal masses.** *AJNR Am J Neuroradiol* 1996;17:1211–1218
3. Allen RW, Harnsberger HR, Shelton C, et al. **Low-cost high-resolution fast spin-echo MR of acoustic schwannoma: An alternative to enhanced conventional spin-echo MR?** *AJNR Am J Neuroradiol* 1996;17:1205–1210
4. Weissman JL. **Hearing loss.** *Radiology* 1996;199:593–611
5. Takehara Y, Ichijo K, Tohyama N, et al. **MR cisternography using "long echo train length fast spin echo sequence" for demonstrating the inner ear.** *Nippon Acta Radiol* 1993;53:859–861
6. Phalps PD. **Fast spin echo in otology.** *J Laryngol Otol* 1994;108: 383–394
7. Tien RD, Feisberg GJ, MacFall J. **Fast spin-echo high-resolution MR imaging of the inner ear.** *AJR Am J Roentgenol* 1992;159: 395–398
8. Rubin JB, Enzmann DR. **Imaging of spinal CSF pulsation by 2DFT MR: significance during clinical imaging.** *AJR Am J Roentgenol* 1987;148:973–982
9. Naganawa S, Yamakawa K, Fukatsu H, et al. **High-resolution T2-weighted MR imaging of the inner ear using a long echo-train-length 3D fast spin-echo-sequence.** *Eur Radiol* 1996;6:369–374
10. Takehara Y, Ichijyo K, Tooyama N, Kodaira N, Fujiwara T, Nozaki A. **Three-dimensional projection images of the labyrinth acquired with multislab 3DFT fast spin-echo sequence and dual-array surface coil.** *AJR Am J Roentgenol* 1995;165:645–646
11. Naganawa S, Itoh T, Fukatsu H, et al. **Three-dimensional fast spin-echo MR of the inner ear: ultra-long echo train length and half-Fourier technique.** *AJNR Am J Neuroradiol* 1998;19: 739–741
12. Naganawa S, Senda K, Ishigaki T, et al. **High resolution MR imaging of the inner ear apparatus using 3D-fast spin echo sequence.** *Nippon Acta Radiol* 1995;55:81–82
13. Naganawa S, Ito T, Fukatu H, et al. **MR cisternography of the cerebellopontine angle using 3D fast SE.** *Radiology* 1996; 201(P):–450
14. Kollias S, Samara C, Wichimann W, et al. **High resolution anatomy and pathology of the inner ear using a long echo-train length (ETL), 3D, fast spin echo sequence.** *Proc Int Soc Magn Reson* 1996;1:–635
15. Czerny C, Rand T, Gstoettner W, Woelfl G, Imhof H, Trattnig S. **MR imaging of the inner ear and cerebellopontine angle: comparison of three-dimensional and two-dimensional sequences.** *AJR Am J Roentgenol* 1998;170:791–796
16. Fujita N, Hirabuki N, Kashiwagi N, Watanabe Y, Nakamura H. **Epidermoid tumor of the cerebellopontine angle: signal loss in the contralateral cistern.** *AJNR Am J Neuroradiol* 1998;19: 333–335
17. Casselman JW, Kuhweide R, Deimling M, Ampe W, Dehaene I, Meeus L. **Constructive interference in steady state-3DFT MR imaging of the inner ear and cerebellopontine angle.** *AJNR Am J Neuroradiol* 1993;14:47–57
18. Kurucay S, Schmalbrock P, Chakeres DW, Keller PJ. **A segment-interleaved motion compensated acquisition in the steady state (SIMCAST) technique for high resolution imaging of the inner ear.** *J Magn Reson* 1997;7:1060–1068
19. Enzmann DR, Rubin JB, Wright A. **Use of cerebrospinal fluid gating to improve T2-weighted images.** *Radiology* 1987;162: 763–767
20. Enzmann DR, Rubin JB, DeLaPaz R, et al. **Cerebrospinal fluid pulsation: benefits and pitfalls in MR imaging.** *Radiology* 1986; 161:773–778